Bulletin of the Seismological Society of America, Vol. 81 2, pp. 399-422, April 1991

SEISMIC CHARACTERISTICS OF EARTHQUAKES ALONG THE OFFSHORE EXTENSION OF THE WESTERN TRANSVERSE RANGES, CALIFORNIA

BY ALLISON L. BENT AND DONALD V. HELMBERGER

ABSTRACT

The short- and long-period body waves of five moderate (M_L 5 to 6) earthquakes that took place in the nearshore region of southcentral California between 1969 and 1981 are modeled to obtain the source parameters. Both regional *Pnl* waveforms and teleseismic *P* waveforms are used in this analysis. Four of the events are thrust earthquakes with strikes that rotate southwestward as the epicenters move southward; the fifth is a strike-slip event occurring on a fault subparallel to the San Andreas fault. The focal mechanisms for all five events are consistent with known faults in the source localities and suggest that the regional stress field is compressional in a north-south direction. At least three events have complex source time histories, suggesting that complex sources are common even for events of this size. The most exotic event started with a low stress drop subevent, ruptured bilaterally, and concluded with strong asperity ruptures at each end.

Since *Pnl* waveforms for thrust events are particularly sensitive to crustal thickness, regionalized crustal models were developed. The crustal thickness appears to increase southward but may be a function of the distance of the event from shore rather than of latitude. Basin and range paths yield the thinnest crustal models, while paths crossing the Colorado Plateau and Rockies yield the thickest. We also examined amplitude variations with station and path. In general, the amplitudes seem to be controlled by the station site rather than the path.

INTRODUCTION

In terms of seismic hazard for central and southern California, the role of the offshore region is not completely understood but may be very important. Large earthquakes, such as the 1812 and 1925 Santa Barbara (M_L 6 +) and 1927 Lompoc (M_L 7 +) earthquakes, have occurred in this region in the past and could presumably occur in the future. While large earthquakes are the most damaging, they are infrequent and, in this region, not well recorded since they occurred before the installation of the worldwide networks. Moderate earthquakes (M_L 5 to 6), however, are more frequent and can provide much useful information about the seismic nature of the region.

Determining the source characteristics of these moderate events has two other important contributions. First, these events have been recorded by stations that also recorded the previously mentioned historic events. Thus, these modern events can be used as master events in both locating and determining the characteristics of the older events, and they have been used in a study of the 1927 Lompoc earthquake by Helmberger *et al.* (1990). Secondly, regional observations of these modern events can be used to calibrate complex paths and study regional Green's functions if the source parameters of these events are known. Such studies are becoming increasingly important with the advent of IRIS stations. In this study, we will concentrate on the body waves of five moderate

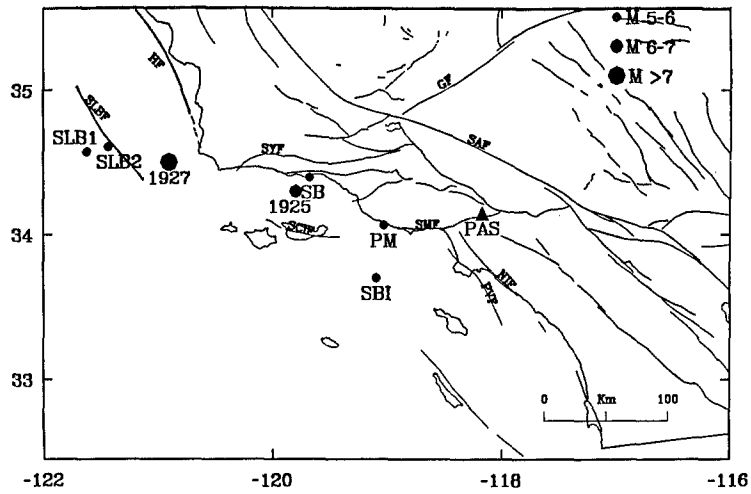

FIG. 1. Map of recent and historic earthquakes in the western Transverse Ranges nearshore region. The symbol size increases with each order of magnitude. SLB1 and SLB2 are the Santa Lucia Banks earthquakes, SB is Santa Barbara, PM is Point Mugu, and SBI is Santa Barbara Island. The historic events are labeled by date. The 1927 earthquake location is that of Helmberger *et al.* (1990). The faults are abbreviated as follows: SAF = San Andreas fault, GF = Garlock fault, SYF = Santa Ynez fault, NIF = Newport-Inglewood fault, SMF = Santa Monica fault, SLBF = Santa Lucia Banks fault, HF = Hosgri fault, PVF = Palos Verdes fault, and SCIF = Santa Cruz Island fault.

earthquakes—the 1981 Santa Barbara Island (M_L 5.3), 1978 Santa Barbara (M_L 5.1), 1973 Point Mugu (M_L 6.0), and two 1969 Santa Lucia Banks events (M_L 5.4, 5.8)—all of which occurred in the offshore extension of the western Transverse Ranges (Fig. 1), to determine their source parameters.

While most of California is dominated by northwest–southeast-trending features, the Transverse Ranges of southcentral California are a series of east–west-trending thrust-faulted mountains. The Los Angeles basin comprises the southern boundary of this region. Both thrust and strike-slip faulting commonly occur in the Los Angeles basin. Strike-slip faulting tends to occur on northwest and north-northwest-striking right-lateral faults, in particular on the Whittier, Newport-Inglewood, and Palos Verdes faults. Notable strike-slip events in the Los Angeles area include the 1933 Long Beach earthquake (M_L 6.3) and the largest aftershock of the 1987 Whittier Narrows earthquake (M_L 5.4). The thrust faults generally strike more or less east–west and dip to the north. The northern boundary of the Los Angeles basin is formed by thrust faults including the Santa Monica and Sierra Madre faults. Thrust faulting also occurs further south in the basin in the Elysian Park and Torrance-Wilmington fold and thrust belts. Thrust events of note in the Los Angeles area include the 1971 San Fernando (M_L 6.6) and 1987 Whittier Narrows (M_L 5.9) earthquakes. A more comprehensive description of earthquakes and faults in the Los Angeles basin can be found in Hauksson (1990).

North and west of the Los Angeles basin lie the Ventura basin and its offshore extension, the Santa Barbara Channel. This region contains the Santa Ynez Mountains and is dominated by east–west-trending thrust faults including the Santa Ynez, Red Mountain, and Santa Cruz Island faults. A number of smaller thrust faults beneath the Santa Barbara Channel have also been

identified by Yerkes *et al.* (1980). The 1812 and 1925 earthquakes which occurred in this region are both believed to have been thrust events (Toppozada *et al.* 1981). The 1978 Santa Barbara earthquake is also a thrust event.

The northern boundary of the Transverse Ranges is marked by the Santa Maria basin and the San Simeon–Hosgri fault zone. There is considerable debate about whether the Hosgri fault is a strike-slip or thrust fault or both (strike-slip in the north and thrust in the south). Discussions of the Hosgri fault zone can be found in Crouch *et al.* (1984), Davis and McIntosh (1987), Hornafius *et al.* (1986), Luyendyk *et al.* (1980, 1985), and Steritz (1986). Most of the larger earthquakes in this region have occurred offshore. The 1927 Lompoe earthquake was a thrust event on a roughly northwest-striking fault offshore west of Point Arguello (Helmberger *et al.*, 1990). Both of the 1969 Santa Lucia Banks earthquakes were also northwest-striking thrust events.

In this study, we use regional and teleseismic data recorded by the WWSSN and Canadian networks to model the earthquakes. Because the earthquakes occurred to the west of most California stations, the data recorded by local arrays do not provide good azimuthal coverage. By using worldwide data we are able to improve the azimuthal coverage, although data to the southwest are still lacking. We hand digitize the data and match the waveforms and amplitudes to synthetic seismograms obtained by a forward modeling technique discussed in detail by Langston and Helmberger (1975) for teleseismic waveforms and by Helmberger and Engen (1980) for *Pnl* waveforms. These techniques provide the faulting parameters, depth of hypocenter, source time history, and seismic moment. The crustal structure used in the teleseismic studies is given in Table 1, where the crustal thickness is allowed to vary as a function of event. A single crustal layer was used in the *Pnl* waveform modeling as displayed in Table 2.

Santa Lucia Banks Earthquakes

In 1969, two moderate earthquakes occurred in the Santa Lucia Banks region. The first, with an estimated M_L of 5.4 (Gawthrop, 1978), occurred on 22 October. The second (M_L 5.8; Gawthrop, 1978) occurred on 5 November. We will refer to these events as SLB1 and SLB2, respectively.

TABLE 1

Teleseismic Velocity Model

Layer	*P* Velocity (km/sec)	*S* Velocity (km/sec)	Density (g/cm^3)	Thickness (km)
1	3.5	2.1	1.6	2
2	6.2	3.5	2.7	22–30
3	8.2	4.5	3.4	

TABLE 2

Regional Velocity Model

Layer	*P* Velocity (km/sec)	*S* Velocity (km/sec)	Density (g/cm^3)	Thickness (km)
1	6.2	3.5	2.7	24–42
2	8.2	4.5	3.4	

At long periods, the waveforms for both events at stations that recorded both are almost identical, suggesting similar source parameters. At short periods, the waveforms for SLB2 are somewhat more complex than those for SLB1 (Fig. 2), indicating that either SLB2 has a complex source time history or that there is some difference in the very near-source structure between the two hypocenters. The former is the more likely cause of the observed waveform complexity since the two events are separated by less than 15 km.

The regional and teleseismic data and synthetic seismograms for these events are shown in Figures 3, 4, 5, and 6. Figure 4 also illustrates the improvement in the fit of the teleseismic waveforms to the data if a low-velocity near-surface

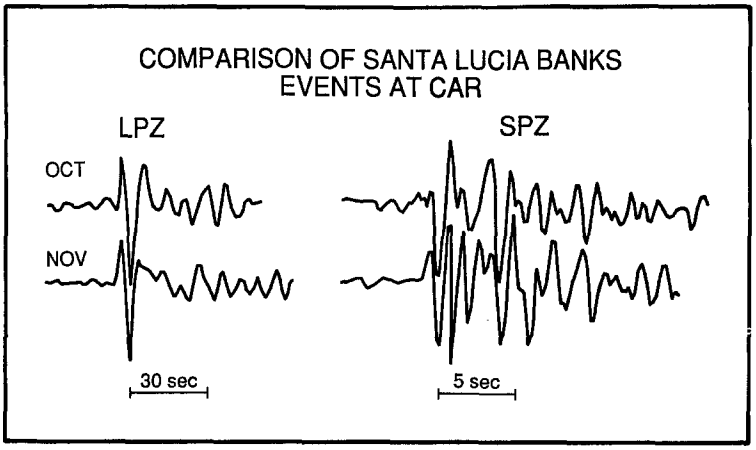

FIG. 2. Long- and short-period data of the Santa Lucia Banks earthquakes recorded at Caracas.

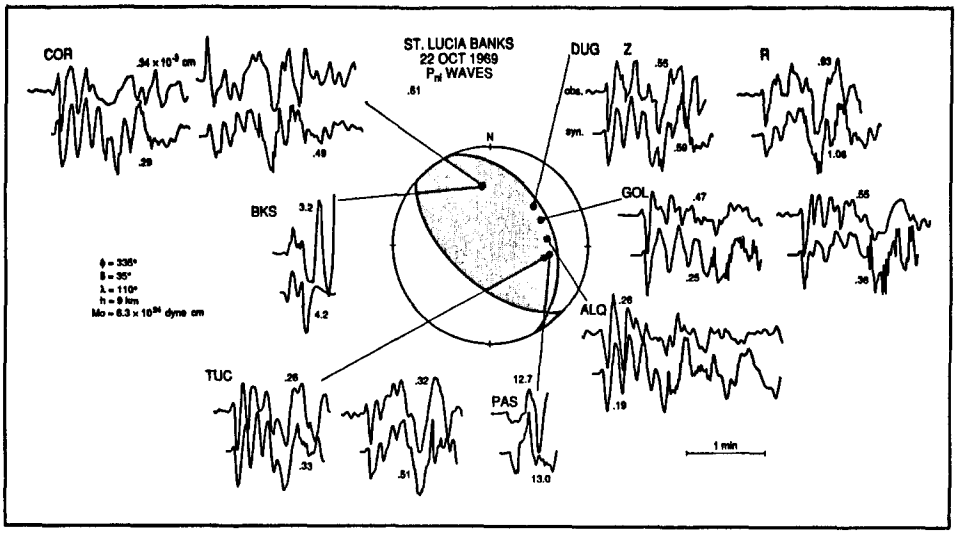

FIG. 3. Regional data and synthetics for the October Santa Lucia Banks event. The upper trace is the data and the lower is the synthetic. When more than one component is available, the vertical is shown on the left and the radial on the right. The seismograms have been normalized to the same maximum peak-to-peak amplitude. Amplitudes are given in units of 10^{-3} cm and have the instrument magnification removed.

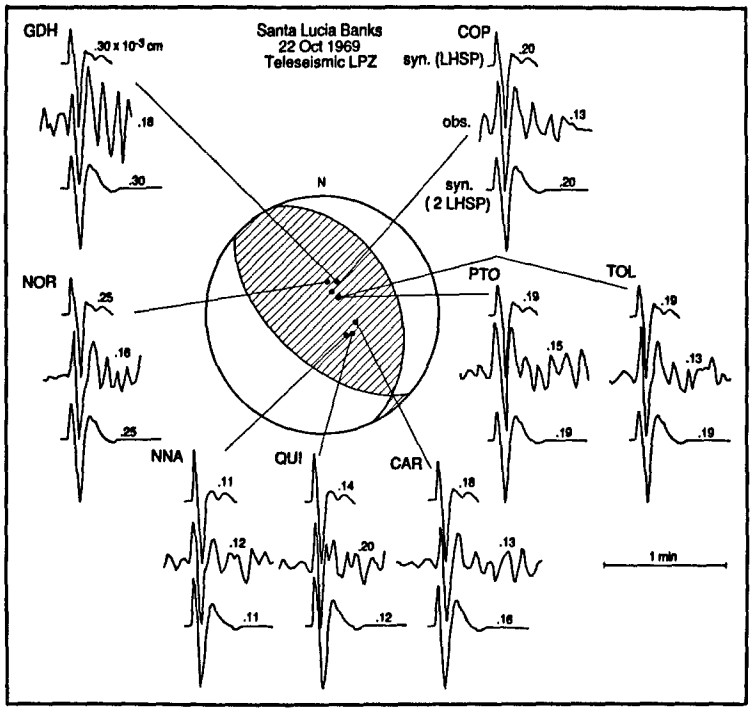

FIG. 4. Teleseismic *P* data and synthetics for the October Santa Lucia Banks earthquake. Only the vertical component is shown. The upper trace is the synthetic for the single layer over half-space model shown in Table 2; the middle is the data; the lower trace is the synthetic for the 2 layer over half-space model shown in Table 1. The amplitudes are given as in Figure 3.

layer is included in the velocity model. The source parameters except for seismic moment are similar for both events. For both we obtain a strike of 335° and rake of 110°. SLB1 has a dip of 35° and depth of 9 km, while SLB2 has a dip of 38° and a depth of 8 km. The long-period seismic moment for SLB1 is 6.3×10^{24} dyne cm; SLB2 has a long-period moment of 1.3×10^{25} dyne cm, roughly twice that of SLB1. The strikes of both events are consistent with that of the Santa Lucia Banks fault zone (Fig. 1).

Figure 7 shows the short-period data and synthetics for SLB1. A triangular source time function with a 0.75 sec rise time and a 0.25 sec fall-off was used to make the synthetics. In general, the fit of the synthetic waveforms to the data is very good. In some cases the synthetic *P* arrival is too sharp. This can be corrected by increasing the rise time, but using a longer source time function worsens the overall fit by increasing the period of the waves. The solution we have used represents the best compromise between amplitude and frequency. The short-period moment is 1.9×10^{24} dyne cm, or 30 percent of the long-period moment.

At short periods, SLB2 (Fig. 8) can be modeled by three subevents with identical focal mechanisms that are the same as the long-period solution. The first two occurred at a depth of 6 km and the third at 4 km. The first and third subevents have approximately equal moments, while the second one is 1.5 to 2 times larger; small changes in the size of this subevent result in only minor variations in the waveforms. All subevents have a duration of 1 sec. The first subevent has a rise time of 0.25 sec and fall-off of 0.75 sec, while the other two

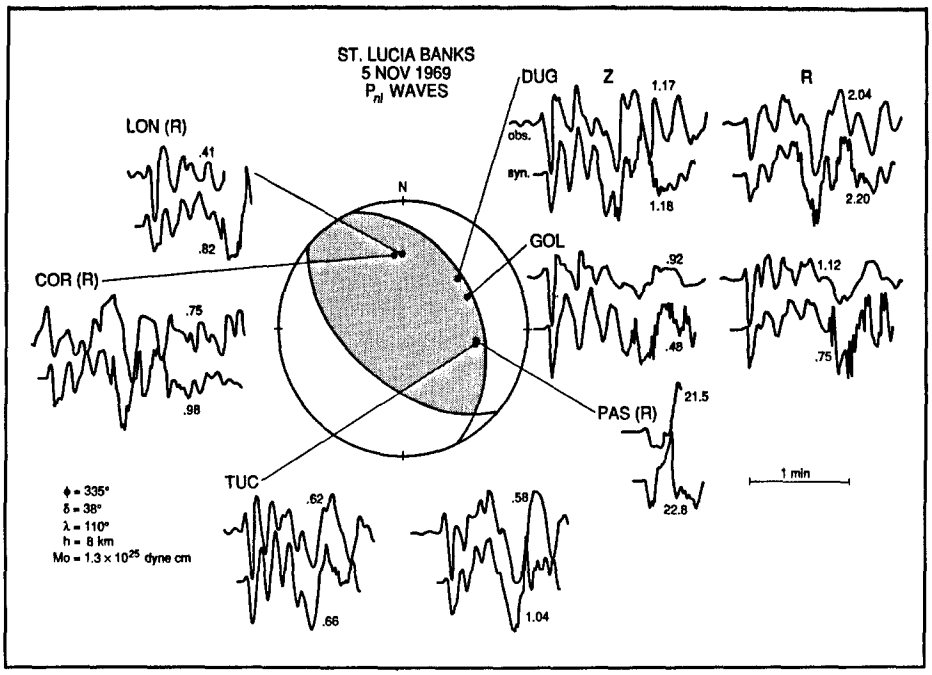

FIG. 5. Regional data and synthetic seismograms for the November Santa Lucia Banks earthquake. The format is the same as Figure 3.

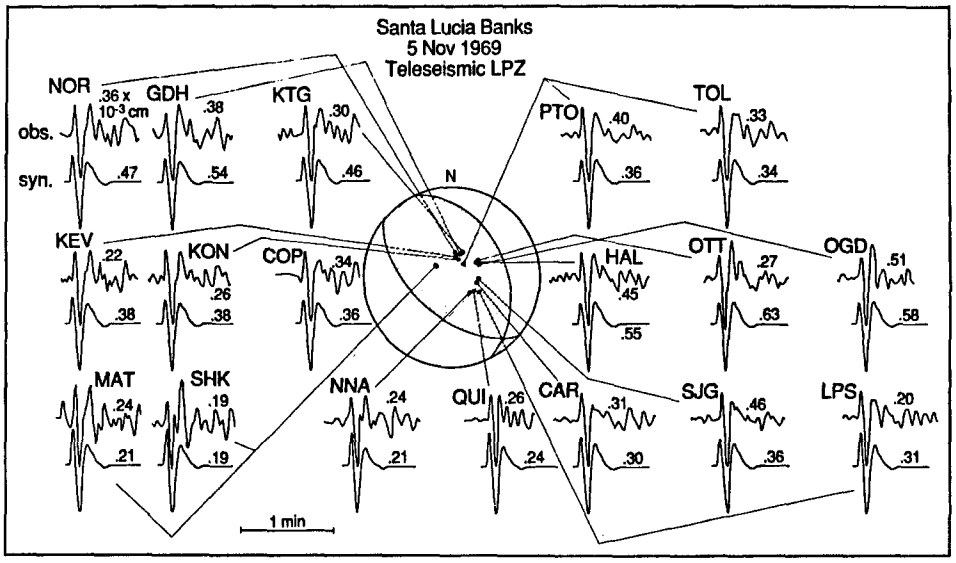

FIG. 6. Teleseismic P data and synthetics for the November Santa Lucia Banks earthquake. The format is the same as Figure 3.

subevents can be modeled with a 0.5 sec rise and fall-off time. The sum of the short-period moments is 47 percent of the long-period moment or 5.2×10^{24} dyne cm. The temporal separation of the subevents varies from station to station suggesting that the subevents are separated spatially. We can deter-

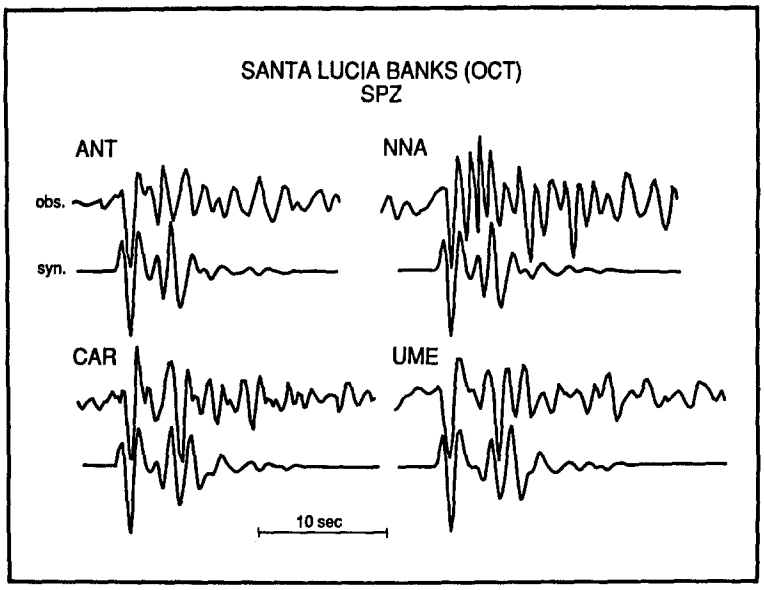

FIG. 7. Short-period data and synthetics for the October Santa Lucia Banks earthquake. The synthetics were calculated using a source time function of $\delta t_1 = 0.75$, $\delta t_2 = 0$, and $\delta t_3 = 0.25$ sec.

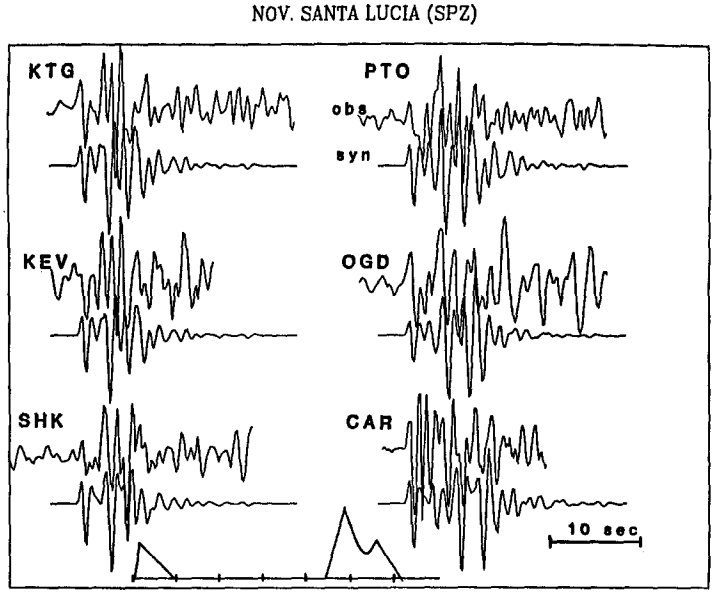

FIG. 8. Short-period data and synthetics for the November Santa Lucia Banks earthquake. The stations are arranged clockwise according to azimuth. The time function is shown (*bottom*) with tic marks at 1 sec intervals.

mine the source separation using the equation (Ben-Menahem *et al.*, 1965)

$$\Delta t = T_0 - D\cos(\phi_0 - \phi)P,$$

where Δt is the observed time difference between the subevents at a station, T_0 is the source time difference of the subevents, D is the spatial separation of the

TABLE 3

STATION PARAMETERS FOR SLB2

Station	Δt_1 (sec)	Δt_2 (sec)	ϕ (°)	P (km/sec)$^{-1}$
CAR	5.7	1.0	102.1	0.065
KEV	2.8	0.7	10.9	0.053
KTG	2.8	0.8	22.3	0.062
OGD	4.2	1.0	65.8	0.077
PTO	3.7	0.8	44.5	0.047
SHK	3.0	0.5	306.9	0.047

Δt_1 is the separation between the first and second subevents. Δt_2 is the separation between the second and third subevents.

subevents, ϕ_0 is the azimuthal separation of the subevents, ϕ is the station azimuth, and P is the ray parameter. The station parameters are summarized in Table 3. The second subevent occurred 4.4 sec after the first and was 36 km away with an azimuthal separation of 340°—more or less along the strike of the fault. The third subevent occurred 0.7 sec after the second and was located 4 to 4.5 km almost due west (272°) of it. The short-period records can be read with an uncertainty of less than 0.2 sec, which results in a distance error of less than 5 km in the spatial separation of the subevents. Modeling the long-period records with this solution we obtain a combined moment of 2.2×10^{25} dyne cm, or 5.5×10^{24} for the first and third subevents and 1.1×10^{25} for the second.

The rupture velocity should be equal to D/T_0. For this earthquake, the apparent rupture velocity is 8 km/sec, which is not physically reasonable (rupture velocities are normally less than the shear velocity), suggesting that the earthquake did not occur as a single propagating rupture. The large spatial separation and small time separation may imply that the second subevent was triggered by the first subevent. More data, particularly from South America and Asia where the subevents have maximum and minimum time separations respectively, would help verify the triggering hypothesis. An alternate explanation is that the rupture began with a small subevent spatially located between the two subevents (but closer to subevent 1) and then propagated bilaterally. Because this subevent is not seen teleseismically, it must be a low stress drop event with a seismic moment smaller than that of the other subevents. If this subevent has a thrust mechanism, we would expect the seismic moment to be less than 5×10^{24}, as earthquakes with moments greater than this are usually recorded teleseismically. If it has a strike-slip mechanism, then it could have a moment as high as 10^{25} dyne cm and not be seen at teleseismic distances (see also the discussion of the Santa Barbara Island earthquake).

In modeling the short-period records, the first arrivals were found to be later than expected based on the Caltech catalog location and origin time for SLB2. Further inspection showed that direct P was consistently about 5.5 sec late at all stations. We also timed the corresponding long-period records and found the same travel-time difference but with a bit more scatter in the data. Since we have good azimuthal coverage (180°) for this event, the consistency of the differences between the theoretical and observed travel times at all stations suggests that the origin time is more likely to be the cause of the error than is the location. The ISC catalog lists the USGS origin time as 5.7 sec later than the PAS time. The PAS and USGS locations are also slightly different, but not

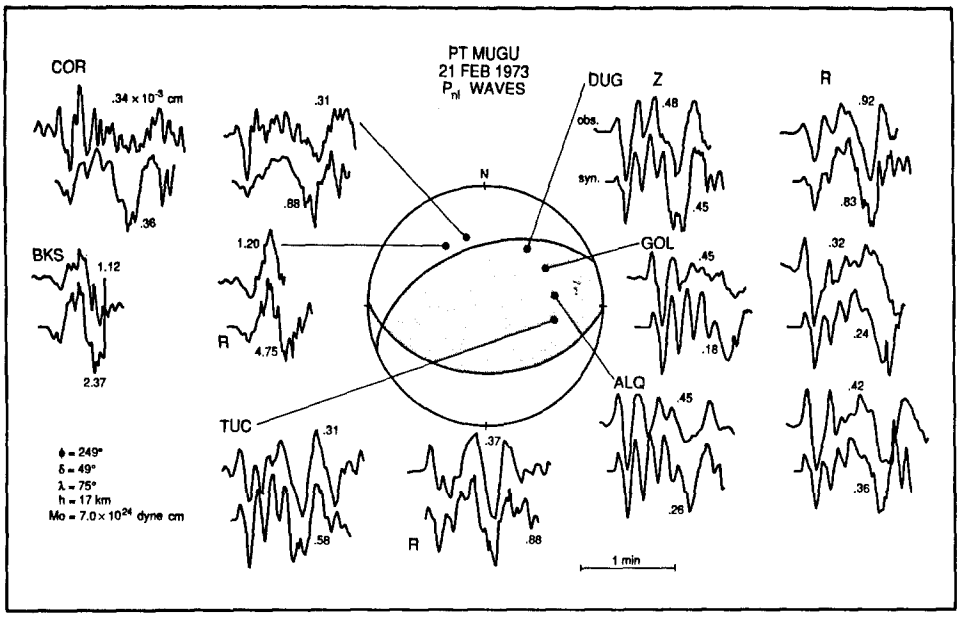

FIG. 9. Regional long-period data and synthetics for the Point Magu earthquake. The format is the same as Figure 3.

by enough to compensate for the difference in origin times. The USGS origin time is more consistent with the observed arrival times. The teleseismic travel times suggest that either the PAS origin time is incorrect or that the PAS origin time reflects the unseen subevent referred to in the previous paragraph, while the USGS origin time is based on the first subevent seen teleseismically.

POINT MUGU

The Point Mugu earthquake of 21 February 1973 (M_L 6.0; Ellsworth *et al.*, 1973) is the deepest of the events studied, occurring at a depth of 17 km. It is primarily a thrust event with a strike of 249°, dip of 49°, and rake of 75°. This mechanism is in good agreement with that of Ellsworth *et al.* (1973) obtained from local first-motion data. The regional and teleseismic waveforms are shown in Figures 9 and 10, respectively. The north-dipping nodal plane is well constrained by the observed first motions. While the first motions at COR and EDM are somewhat ambiguous, DUG and SES are definitely compressional, and BKS and VIC are definitely dilatational. We did not model EDM, SES, and VIC because they are located at upper mantle triplication distances, which are more suited for modeling velocity structures than for source studies. Nevertheless, the first motions at these stations were useful in constraining the focal mechanism. The auxiliary plane is obtained from the rake that best fits the overall waveforms. The fault parameters suggest that the earthquake occurred on the westward extension of the Santa Monica fault (Ellsworth *et al.*, 1973; our Fig. 1). We obtain a long-period seismic moment of 7×10^{24} dyne cm. The scatter of the amplitude ratios of the data to synthetics is somewhat larger for this event than for the other four but is not improved by altering any of the source parameters.

At short periods the Point Mugu earthquake appears to consist of at least two

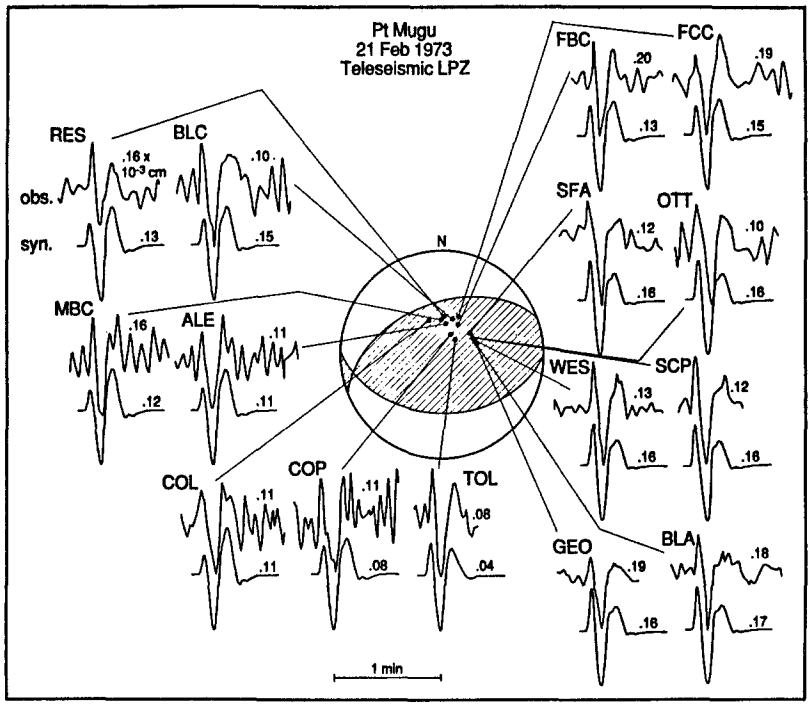

FIG. 10. Long-period teleseismic data and synthetics for the Point Mugu earthquake. The format is the same as Figure 3.

subevents. Within the resolving capabilities of the data, both subevents appear to have identical focal mechanisms and source time functions. The focal mechanisms are the same as that obtained for the long-period records, and the subevents can be modeled with triangular source time functions of 1 sec duration each. Both subevents occurred at a depth of 14 km, and, since there is no apparent azimuthal dependence on the source time separation, the subevents must be located very close together spatially. The second subevent occurred 0.85 sec after the first and had a moment that was 1.5 times larger. The short-period moment is 6.5×10^{24} dyne cm and only slightly less than the long-period moment. A few stations, TOL and ALE in particular, are better modeled by three subevents, with the third, roughly the same size as the second, occurring 4.25 sec after the first. This apparent complexity is possibly the result of near-receiver structure. ALE is on an island and near the coast, and TOL may have near-receiver structural complexity as exhibited by the more abundant and larger late arrivals than other stations for the Santa Barbara as well as the Point Mugu event. The short-period data and synthetic seismograms are shown in Figure 11. Using the two source solution to model the long-period records, we obtain seismic moments of 2.9×10^{24} and 4.3×10^{24} dyne cm for the first and second subevents respectively.

In an earlier study of S waves recorded by strong-motion instruments, Boore and Stierman (1976) also found evidence that the Point Mugu earthquake was a double event, with the same time separation indicated by the teleseismic records. The waveforms at one particular station, Port Hueneme, suggest that either the second subevent has a different focal mechanism than the first or

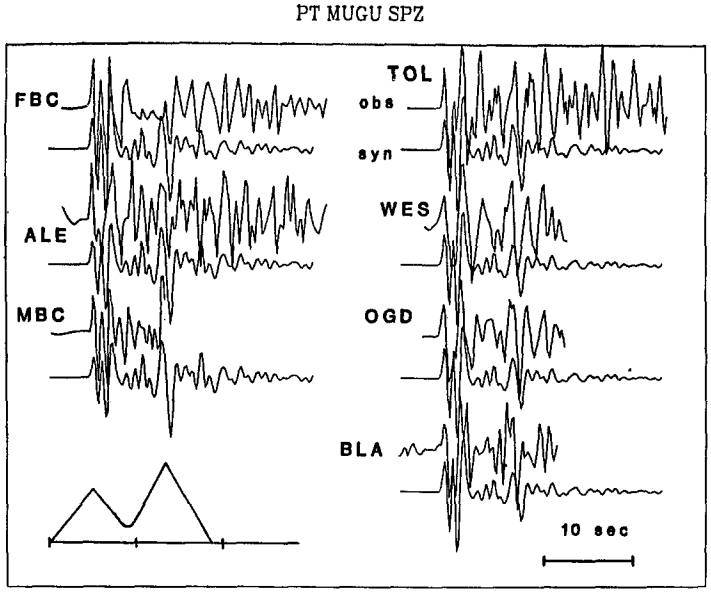

FIG. 11. Short-period teleseismic data and synthetics for the Point Mugu earthquake.

that it is smaller. Both of these interpretations disagree with out results obtained from the short-period records. Changing only the relative size of the subevents produced waveforms that were compatible with neither the teleseismic nor the strong-motion waveforms. Teleseismic P waves from thrust events are not very sensitive to changes in the focal mechanism (Bent and Helmberger, 1989; Langston, 1978), implying that, although the data do not require different focal mechanisms for the two subevents, such a solution cannot be completely ruled out. In an attempt to reconcile the teleseismic and local observations, we have investigated the possibility of nonidentical subevents. Since aftershocks of this earthquake included both thrust and strike-slip events (Ellsworth *et al.*, 1973), both types of solutions were tried. We altered only the second subevent because the first-motion solution agreed with the solution obtained by modeling. The results are shown in Figure 12. We also tried adjusting the time function, which can be related to stress drop, of the second subevent. If the second subevent has a shorter rise time than the first subevent (Fig. 12b), the teleseismic waveforms fit better at the beginning of the record. Increasing the rise time of the second subevent (Fig. 12c) improves the fit of the strong-motion synthetics but worsens the fit at teleseismic distances. For the second subevent, we tried focal mechanisms that resulted in a near nodal direct SH at Point Hueneme. These solutions would allow the second subevent to appear smaller than the first at this station. A pure thrust solution with a strike of 295° did not adversely affect the teleseismic waveforms (Fig. 12d). A strike-slip mechanism did not produce satisfactory results (Fig. 12e). In light of the aftershock distribution of the Point Mugu earthquake (Ellsworth *et al.*, 1973; Boore and Stierman, 1976), a 50° rotation in strike does not seem unreasonable.

SANTA BARBARA

The 13 August 1978 M_L 5.1 (Hutton *et al.*, 1985) Santa Barbara earthquake is an oblique thrust event that occurred at a depth of 12 km. The fault

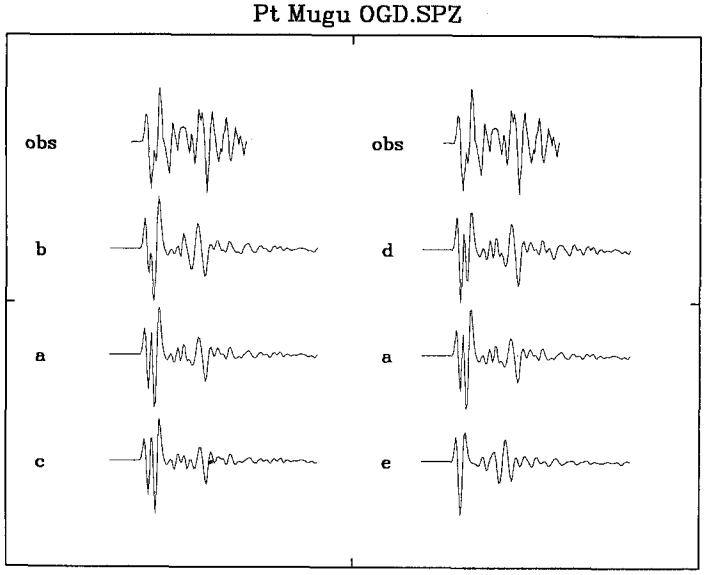

FIG. 12. Short-period records for Point Mugu recorded at OGD. The data is shown at the top of each column. The synthetics consist of two subevents. The first subevent is as described in the text. In all cases $M_{0_2} = 1.5M_{0_1}$. The second subevent is as described in the text with the following modifications: (a) no change; (b) $\delta t_1 = 0.25$, $\delta t_3 = 0.75$; (c) $\delta t_1 = 0.75$, $\delta t_3 = 0.25°$; (d) strike = 295, dip = 45°, rake = 90°; and (e) strike = 245°, dip = 90°, rake = 180°.

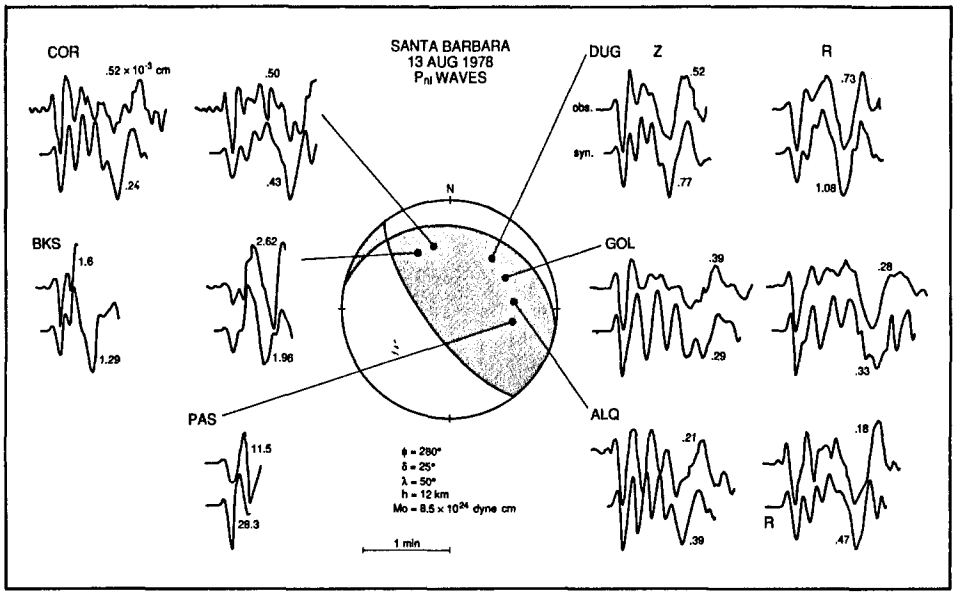

FIG. 13. Long-period regional data and synthetics for the Santa Barbara earthquake. The format is the same as Figure 3.

parameters are well constrained by the regional data (Fig. 13). We obtain a strike of 280°, dip of 25°, and rake of 50°. This earthquake was also modeled by Wallace *et al.* (1981a), who obtained a strike of 295°. We found that their strike resulted in a *Pn* amplitude that was too small at stations to the north (BKS and

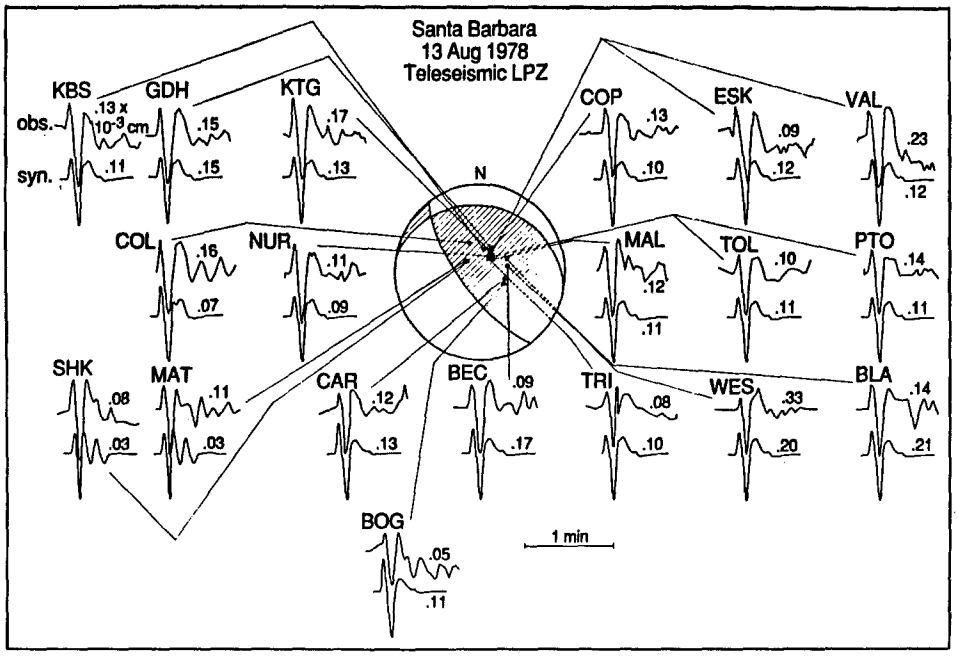

FIG. 14. Long-period teleseismic data and synthetics for the Santa Barbara earthquake. The format is the same as Figure 3.

COR). The synthetics at these stations fit the data even better if we rotate the strike closer to east-west, but this results in a poor fit at other stations (DUG in particular). Our final choice of strike is similar to that obtained from local data (Corbett and Johnson, 1982). It is not clear which fault this earthquake occurred on, but its orientation is consistent with known faults in the region [Corbett and Johnson, 1982; Yerkes *et al.*, 1980]. For this event we obtain a long-period seismic moment of 9.5×10^{24} dyne cm. Teleseismic records were also modeled and the results are shown in Figure 14.

The Santa Barbara earthquake also appears to be a complex event at short periods. The short-period waveforms are best modeled by two subevents separated in time by 1.5 sec (Fig. 15). Some stations are better modeled with slightly longer or shorter (± 0.25 sec) source separations, but the variation is not azimuthally dependent, so it is unlikely to be caused by spatial separation of the subevents. Both have mechanisms identical to the long-period solution and can be modeled with triangular source-time functions: the first with a duration of 0.5 sec and the second with a duration of 1.0 sec. The combined short-period moment is 1.8×10^{24} dyne cm (15 percent of the long-period moment). Although we prefer identical focal mechanisms for both subevents, we cannot completely rule out different sources. Figure 16 illustrates the effect of nonidentical focal mechanisms on the synthetics. Increasing the dip of the second subevent results in smaller arrivals 2.5 and 5.5 sec after the onset of the direct *P* arrival, which worsens the fit of the synthetics. Decreasing the dip has very little effect. Therefore, a small change in dip ($< 10°$) cannot be completely ruled out. Changing the strike of the second subevent has much less of an effect. Rotating the strike southwestward up to 20° has no significant effect; rotating

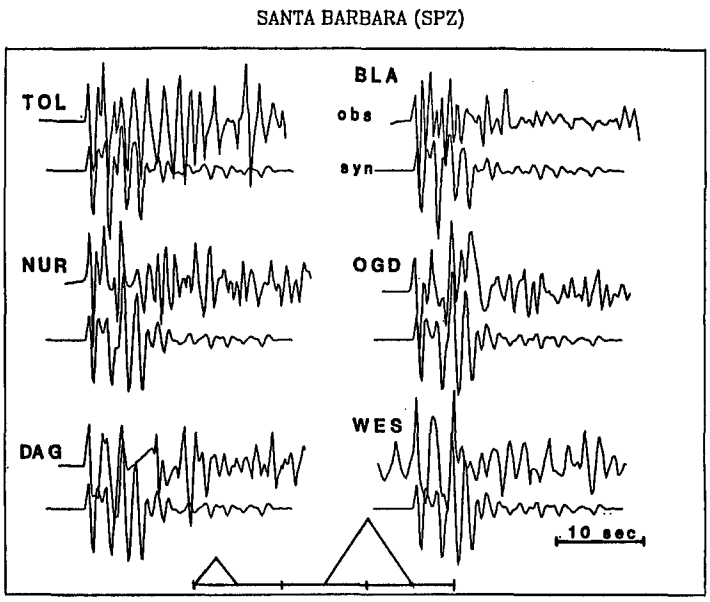

FIG. 15. Short-period teleseismic data and synthetics for the Santa Barabara earthquake.

the strike 20° northwestward has the same effect as increasing the dip. These results suggest that, if there is a strike rotation, it is more likely to be to the southwest than to the northwest. Using our preferred solution to remodel the long-period records, we obtain a seismic moment of 1.1×10^{25} dyne cm or 3.3×10^{24} for the first subevent and 8.1×10^{24} for the second. The first subevent occurred at a depth of 8 km. The second, which was 2.5 times larger than the first, occurred at a depth of 5 km. The depth difference between the subevents suggests that the fault ruptured upward and southward, which is consistent with rupture on the north-dipping plane. The discrepancy between the long- and short-period depths was also observed by Wallace *et al.* (1981a). We interpret the short-period solution to be the rupture of two asperities, while the long-period solution describes the overall rupture process.

There are some good strong-motion records for this earthquake [Wallace *et al.*, 1981a]. The short-period solution described above does not produce satisfactory synthetics at some of these stations. If, instead of using two point sources, we allow the first subevent to be a downward propagating rupture and let the second subevent propagate upward, the fit of the synthetics to the data is much improved. The relative amplitudes of the three components can be further improved if we use the strike of Wallace *et al.* (1981a) or if we move the epicenter about 5.5 km to the north or north-northeast.

SANTA BARBARA ISLAND

The 4 September 1981 Santa Barbara Island earthquake, unlike the other four, is a strike-slip event. This event is also the most southern of the five earthquakes studied and has an M_L of 5.3 [Hutton *et al.*, 1985]. Because only a few stations recorded this event teleseismically, the source parameters were obtained solely by modeling the regional data shown in Figure 17. We obtain a strike of 314°, a dip of 85°, and rake of 180°. The strike is roughly parallel to

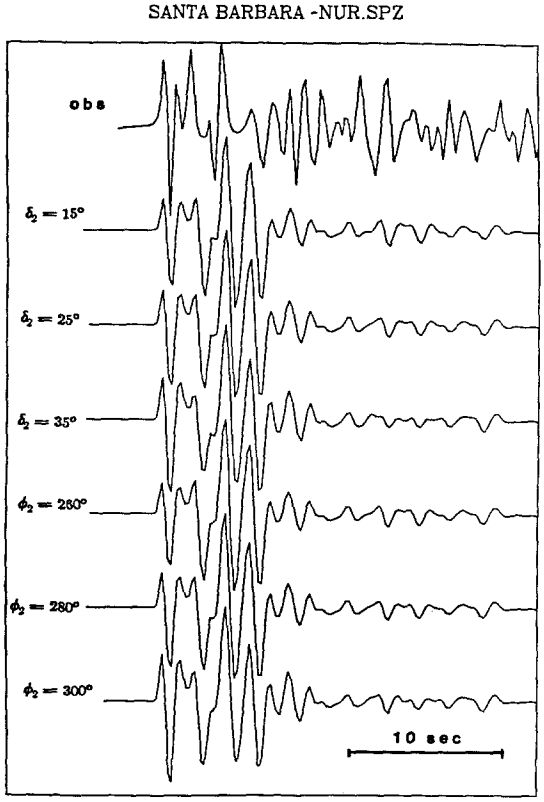

FIG. 16. Short-period data and synthetics for the Santa Barbara earthquake recorded at NUR showing the effect of the focal mechanism on the synthetics. Except for the changes indicated, the synthetics were made using our preferred short-period solution.

the main trend of the San Andreas Fault and also corresponds to that of the Santa Cruz–Catalina Ridge along which the aftershocks of this event lined up and which is believed to be a fault [Corbett, 1984]. Using paleomagnetic and geologic data, Luyendyk *et al.* [1985] classify Santa Barbara Island as part of the Peninsular Range province rather than as part of the Transverse Ranges. The fault plane solution for the Santa Barbara Island earthquake is consistent with this interpretation. The long-period seismic moment is 1.2×10^{25} dyne cm. Even though this event has one of the largest moments of the five events studied here, it was the least well recorded teleseismically. This is not unusual and is related to the radiation pattern associated with strike-slip events. The depth and time function were difficult to determine due to the lack of teleseismic data. Our model used a depth of 11.5 km, which is the depth determined by Corbett (1984). Using this depth we obtain synthetic seismograms which fit the data well, although long-period *Pnl* waves for strike-slip earthquakes are not very sensitive to depth [Helmberger and Engen, 1980], so the depth cannot be well resolved by modeling.

DISCUSSION

Because we have several events relatively close together with respect to regional and teleseismic stations, we can use them to study the stability of a

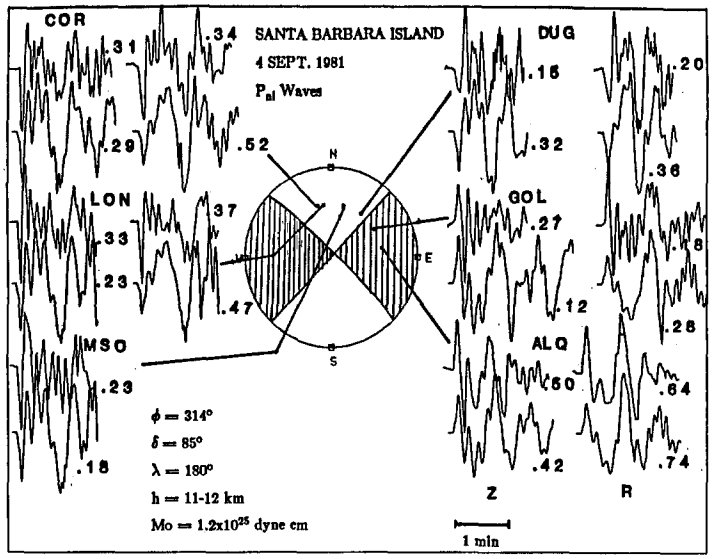

FIG. 17. Long-period regional data and synthetics for the Santa Barbara Island earthquake. The format is the same as Figure 3.

TABLE 4

SUMMARY OF LONG-PERIOD SOURCE PARAMETERS

Event	M_L	Strike (°)	Dip (°)	Rake (°)	Depth (km)	Moment (10^{24} dyne cm)
SLB1	5.4	335	35	110	9	6.3
SLB2	5.8	335	38	110	10	13.0
PM	6.0	249	49	75	17	7.0
SB	5.1	280	25	50	12	9.5
SBI	5.3	314	85	180	11.5	12.0

number of parameters including path and amplitude. Crustal thickness appears to be consistent for both source locations and path. At teleseismic distances, body wave amplitudes are controlled more by site than by azimuth (or lateral variations in the velocity structure). At regional ranges, distance (which can be related to vertical inhomogeneities in the upper mantle) also plays a role. The amplitude and path results will be useful in modeling other events in this region.

Source Properties

The long- and short-period source parameters are summarized in Tables 4 and 5, respectively. In Table 5, all time lags are measured with respect to the onset of the first subevent. The thrust events all have fault plane solutions consistent with known thrust faults in the source region: the Santa Lucia Banks fault, the Santa Monica Fault, and a number of mapped faults in the Santa Barbara Channel region. The strike of the Santa Barbara Island earthquake correlates with that of a known fault related to the Santa Cruz–Catalina ridge. The strikes of the thrust events studied rotate southwestward as the epicenters

TABLE 5

SHORT-PERIOD SOURCE PARAMETERS

Event	Depth (km)	M_0 (10^{24} dyne cm)	δt_1 (sec)	δt_2 (sec)	δt_3 (sec)	Lag (sec)
SLB1	9	1.9	0.75	0.00	0.25	0.0
SLB2.1	6	1.5	0.25	0.00	0.75	0.0
SLB2.2	6	3.1	0.50	0.00	0.50	4.4
SLB2.3	4	1.5	0.50	0.00	0.50	5.1
PM.1	14	2.6	0.50	0.00	0.50	0.0
PM.2	14	3.9	0.50	0.00	0.50	0.85
SB.1	8	0.5	0.25	0.00	0.25	0.0
SB.2	5	1.3	0.50	0.00	0.50	1.5

move southward. If we assume the north-dipping plane is the fault plane, which is consistent with mapped surficial faults in the region [Hauksson, 1990], then the strike rotation corresponds qualitatively to the changing strike of the San Andreas fault in the region of the Big Bend. This suggests that the San Andreas fault controls, at least in part, the stress field in the Transverse Ranges. In general, the focal mechanisms imply compression on a regional scale: northeast–southwest in the Santa Lucia Banks region and north–south elsewhere. Previous measurements and calculations of the stress field in this region give similar results (Hauksson, 1990; Zoback *et al.*, 1987).

Structural Implications

Earlier applications of *Pnl* waveform modeling involved mostly strike-slip events (Wallace *et al.*, 1981b). Variations in source depth as well as crustal thickness produce similar waveforms for this particular focal mechanism and, thus, a single source depth of 8 km embedded in a 32-km-thick crustal layer has proven adequate for modeling these events. Thrust events are more sensitive to crustal thickness and source depth, and significantly better fits are achieved by allowing the crustal thickness to become path dependent. Furthermore, since an array of events are recorded by an array of stations, it becomes possible to examine path stability. The depth of the hypocenter can be constrained from the *pP-P* and *sP-P* times. Once the depth is known we use the *Pl-Pn* time to constrain the crustal thickness. The crustal thickness used to model a given path usually represents the average crustal thickness from source to receiver, but it may be strongly influenced by the near-source or near-receiver structure (Zhao *et al.*, 1990).

The crustal thicknesses used in the *Pnl* modeling are shown in Figure 18. The crustal thickness tends to increase as the epicenters move southward, although the exact value varies from station to station. This trend does not necessarily mean that the crust actually thickens from north to south, since the distance of the epicenter from the coast decreases southward. The apparent thickening may be a reflection of the difference between continental and oceanic crust. One exception to this trend is the station GOL. All four thrust events require a thick crust of 42 km. Santa Barbara Island also requires a thick crust at GOL, but the data can be satisfied by a thickness of 37 km. The paths to GOL all cross the Colorado plateau and southern Rocky Mountains (Fig. 19), and the crustal thicknesses seem to be a result of the near-receiver structure. The path

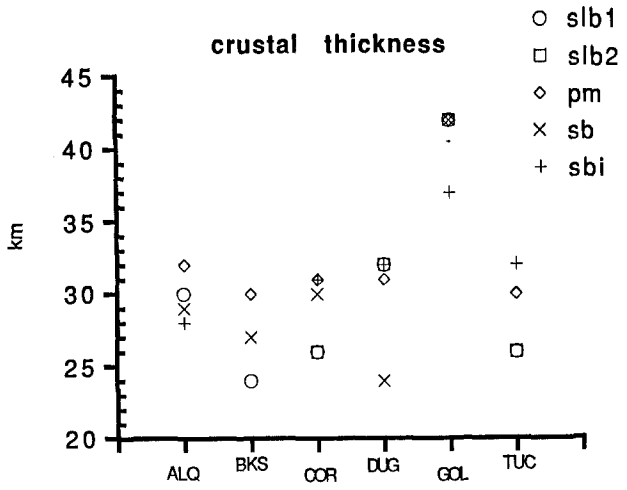

FIG. 18. Crustal thicknesses (in km) that best fit the data. The uncertainty is 1 to 2 km. The events are labeled as in Figure 1.

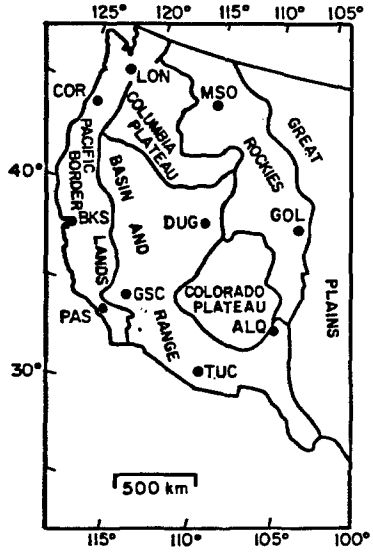

FIG. 19. Map showing stations used in modeling regional phases and their tectonic settings (after Helmberger and Engen, 1980).

from Point Mugu to DUG appears to be anomalously thin. A possible explanation for this is that we are seeing the *Pn* phase from one subevent and the *Pl* from another. Since the strong-motion records suggest that the subevents have different focal mechanisms, this is not an unreasonable interpretation. The Santa Barbara Island data do not consistently follow the southward-thickening trend or the trend of thinning with increasing distance from shore. In general, these data can be satisfied with the initial crustal thickness of 32 km (except at ALQ and GOL), probably indicating that strike-slip events are less sensitive to small changes in crustal thickness than are thrust events, as discussed earlier.

At teleseismic distances, the crustal thickness appears to be largely a function of the near-source structure and does not noticeably vary from one station to another. Again the crust appears to thicken as the epicenters move southward and toward the coast. We use a thickness of 24 km for the Santa Lucia Banks events, 28 km for Santa Barbara, and 32 km for Point Mugu.

Because the same general trends with respect to crustal thickness are seen at both teleseismic and regional distances, and because the greatest difference in the source to receiver path for any given station occurs in the near source region, we have interpreted the crustal thickness variations to be the result of near-source structure. There are, however, other possible explanations. In a similar study of earthquakes in Tibet, Zhao and Helmberger (1990) found a correlation between crustal thickness and *Pn* velocity anomalies. That is, when the crust was thick the upper mantle velocity was slow, and when the crust was thin the velocity was fast. We determined the *Pn* velocity by comparing the observed and theoretical travel times based on the velocity model in Table 2. The resulting velocities were too scattered to be of use in determining a regional velocity structure, but there was no correlation between anomalous crustal thicknesses and anomalous velocities, suggesting that this is not the cause of the observed crustal thickness pattern. We have used a laterally homogeneous flat-layered velocity model. While this model produces good waveform fits, it is a simplified version of the true velocity structure, and it is possible that lateral inhomogeneities or dipping layers in the crust or upper mantle are affecting the apparent crustal thicknesses.

The *Pnl* waveforms, particularly at large distances, can be influenced by gradients in the upper mantle, as illustrated in Figure 20. A positive gradient increases the amplitude of the *Pn* arrival with respect to the later phases. Such a gradient would improve the fit of synthetic seismograms at distant stations to the east—GOL in particular—and, to a lesser extent, some of the stations to the north (Figs. 3, 5, 9, and 13).

Amplitude Stability

In modeling source parameters, large variations, often as large as 50 percent, from the average moment are observed at some stations. Changing the source parameters usually does not reduce the scatter. When seismograms from a large number of stations are available, it is assumed that the calculated moment represents the true seismic moment. If only a few stations are available, as is often the case for smaller and historic earthquakes, the calculated moment may be biased by site or path effects at one station. If a given station is known to consistently imply a moment that is larger or smaller than the average, then this effect can be corrected for. If the scatter in the mismatch is small, an exact correction can be obtained. If only the sign of the mismatch is consistent, then we can only determine whether the calculated moment is likely to be a maximum or minimum estimate.

Since we have modeled a number of earthquakes with almost identical paths with respect to telesesimic stations, we have the opportunity to study the amplitude variations as a function of the station. The amplitudes may be affected by the path, but the effects should be the same for every event. The four thrust events studied were well recorded teleseismically. We examined observations at all stations which recorded three or more of these events, a total of 12 stations—5 teleseismic and 7 regional—and the results are given in Figure 21.

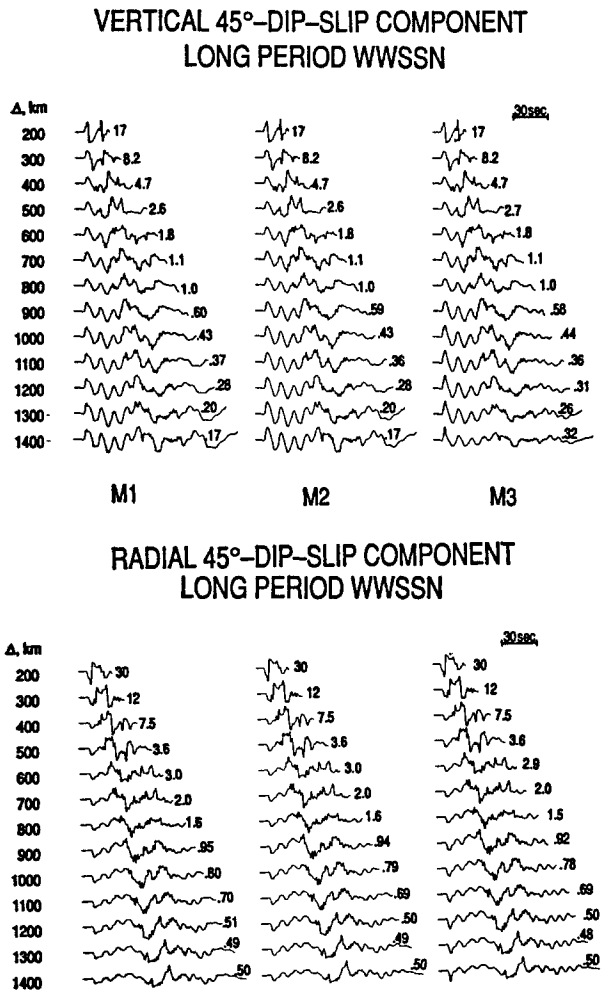

FIG. 20. The 45° dip-slip component of the Green's functions convolved with a long-period instrument response. M2 is for a half-space upper mantle with a velocity of 8.2 km/sec. M1 and M3 are both for two layered mantles for which the upper layer is 100 km thick with a velocity of 8.2 km/sec. In M1 the velocity of the lower layer is 8.1 km/sec and in M3 it is 8.3 km/sec. Amplitudes are in units of 10^{-6} cm. (a) Vertical component; (b) radial component.

At regional distances three stations (ALQ, BKS, and COR) showed a high degree of variability in the ratio of observed and theoretical amplitudes. The synthetic amplitudes at GOL were consistently smaller than the data, although the ratio varied considerably. TUC showed the opposite trend with the synthetics being consistently larger than the data. DUG and PAS usually gave synthetic amplitudes that were close to the observed value, but in each case there was one event which did not. When we add the Santa Barbara Island data, the pattern at GOL remains but DUG appears to be less reliable. Three of the teleseismic stations (COP, PTO, and TOL) show a high degree of scatter. The synthetic amplitudes at CAR, which have a maximum difference of 20 percent from the average, are generally close to the observed amplitudes. At GDH the synthetics tend to be greater than or equal to the data but the actual ratios are more varied than at CAR.

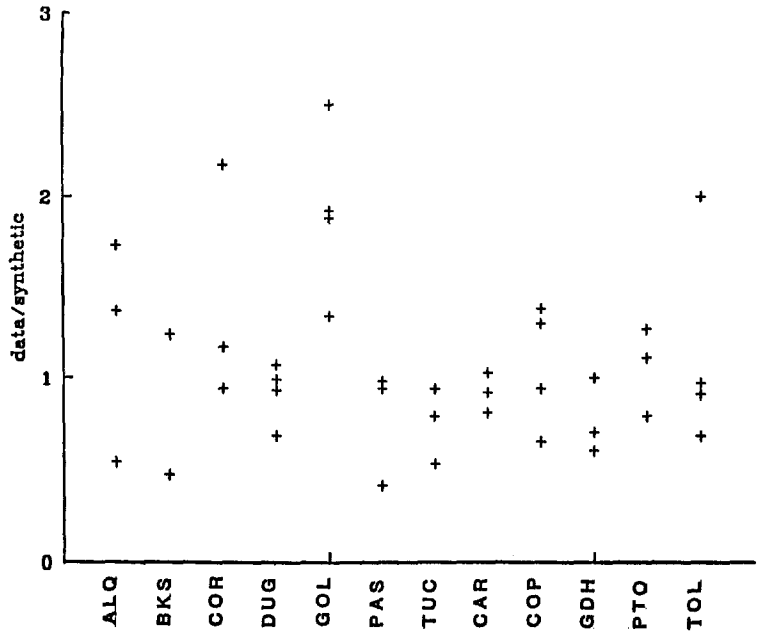

FIG. 21. Ratio of observed amplitudes to synthetic seismograms (vertical component) as a function of station (for PAS we have used the radial component since the vertical was unavailable).

When the teleseismic amplitude ratios are plotted as a function of azimuth using all available station there are some regional trends, but they are not strong enough to be conclusive. Station to the northwest (Japan and Alaska) tend to have synthetic amplitudes less than or equal to the observed amplitudes, but there is a wide range of values. The scatter for South American stations is less than for other regions. The mismatch tends to be small (i.e., the synthetic amplitude is usually close to the observed amplitude), but the synthetic amplitudes are equally likely to be larger or smaller than the data. At stations in the eastern United States and Canada, the synthetics are more likely to be larger than the data, but again there are exceptions to this trend. European and northern Canadian stations show a high degree of scatter in the amplitude ratios. At teleseismic distances, the station site appears to be more important than the path.

We also plotted the amplitude ratio of regional stations as a function of distance, amount of dip-slip, *Pn* velocity, and travel-time residual. Only distance showed any pattern. The lack of any correlation between amplitudes and either velocity or travel-time residual implies that using a laterally homogeneous velocity model is not adversely affecting the outcome of our modeling efforts. Although there is some scatter, the largest data to synthetic amplitude ratios tend to occur at the greatest distances. This pattern is prominent on the vertical component (Fig. 22a), but is not apparent on the radial component (Fig. 22b). This can be predicted from theoretical models. On the vertical component, the contribution from *Pn* relative to *Pl* increases with distance (Fig. 20a), while the *Pl* portion of the record dominates at all distances on the radial component (Fig. 20b). If a positive upper mantle gradient is included in the velocity model, *Pn* becomes even more dominant at large distances where we

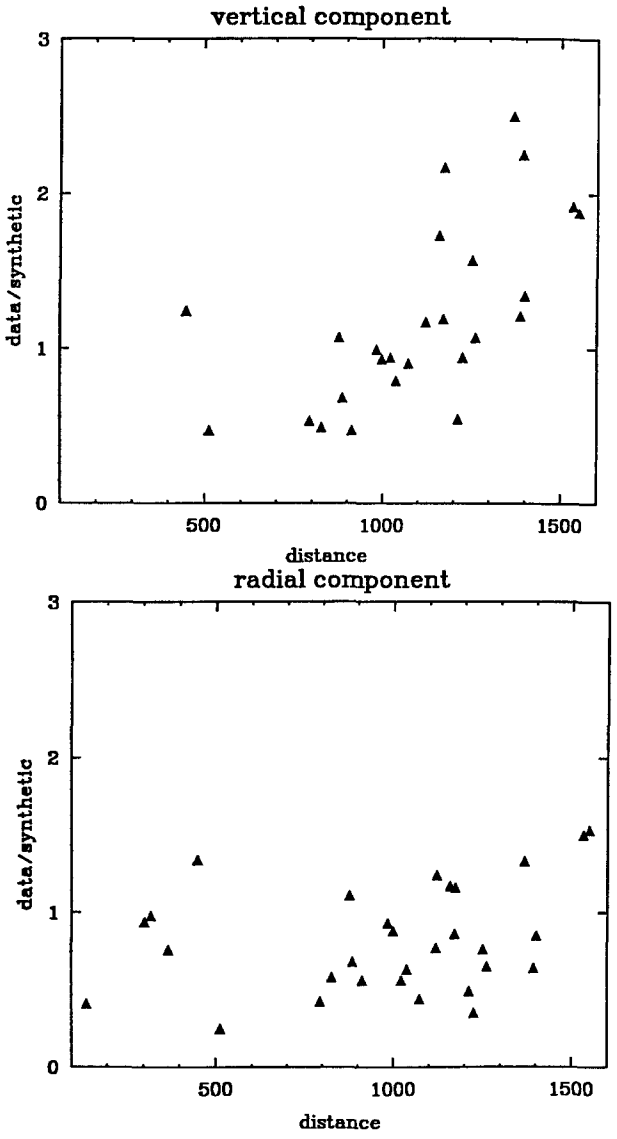

FIG. 22. Ratio of observed amplitudes to synthetic seismograms as a function of distance in km for the (a) vertical and (b) radial components at regional distances.

would expect the upper mantle structure to have a greater effect. Including a gradient increases the amplitude of the vertical synthetics without affecting the radial component (Fig. 22) and explains the amplitude mismatch at larger distances, in particular at GOL.

SUMMARY

In summary, we have found that the nearshore region of south-central California is dominated by thrust faulting. The average strike is roughly east-west, although there is some variation. The fault plane solutions are consistent with a stress field dominated by north-south compression. Complex

sources appear to be fairly common for moderate earthquakes in this region. The fit of the synthetic seismograms to the data was improved by allowing the Green's functions to vary with station and epicentral locations as well as distance. By studying the events as a group, we were able to determine some characteristics of the regional structure and whether amplitude mismatches are consistent at a number of stations and azimuths. Crustal thickness appears to be a function of distance from shore (and possibly latitude). Some individual stations showed consistent mismatches with respect to amplitude, but azimuthal trends were weak at best, suggesting that this is a site rather than a path effect. At *Pnl* distances there was some correlation between amplitude mismatch and distance.

Because historic earthquakes in the western Transverse Ranges were not well recorded regionally, and only somewhat better teleseismically, it is important to know as much as possible about the seismic characteristics of the region to be able to make full use of those records that are available. To locate historic earthquakes, accurate locations and depths of recent events are needed to calibrate paths and travel times; focal mechanisms of historic events can be determined by comparing their waveforms to well-modeled recent events at the same stations; and moments can be determined by comparing amplitude data to recent events. The source parameters and location of the 1927 Lompoc earthquake were determined by Helmberger *et al.* (1990) by using some of the events in this study as master events. These events will also be useful in studying other historic events, such as the 1925 Santa Barbara and 1933 Long Beach earthquakes, in future efforts.

Acknowledgments

This work was supported by USGS Contract 14-08-0001-G1872. California Institute of Technology Division of Geological and Planetary Sciences contribution no. 4931. Hiroo Kanamori read an earlier version of this paper and made some suggestions that improved its quality. Lisa Wald also reviewed the paper and provided us with many helpful comments.

References

Ben-Menahem, A., S. W. Smith, and T. L. Teng, (1965). A procedure for source studies from spectra of long-period seismograms, Bull. Seism. Soc. Am. **55**, 203-235.

Bent, A. L. and D. V. Helmberger (1989). Source complexity of the October 1, 1987, Whittier Narrows earthquake, *J. Geophys. Res.* **94**, 9548-9556.

Boore, D. M. and D. J. Stierman (1976). Source parameters of the Pt. Mugu earthquake of February 21, 1973, *Bull. Seism. Soc. Am.* **66**, 385-404.

Corbett, E. J. (1984). Seismicity and crustal structure studies of southern California: tectonic implications from improved earthquake locations, *Ph. D. Thesis*, California Institute of Technology, Pasadena, Calif., 231 pp.

Corbett, E. J. and C. E. Johnson (1982). The Santa Barbara earthquake of 13 August 1978, *Bull. Seism. Soc. Am.* **72**, 2201-2226.

Crouch, J., S. B. Bachman, and J. T. Shay (1984). Post-Miocene compressional tectonics along the central California margin, in *Tectonics and Sedimentation Along the California Margin*, J. Crouch and S. B. Bachman (Editors), *Pacific Section S. E. P. M.* **38**, 37-54.

Davis, T. L. and K. D. McIntosh (1987). A retrodeformable structural solution across the southern Coast Ranges and implications for seismically active structures, *Geol. Soc. Am. Cordilleran Sect. Meeting, Abst. with Prog.* **19**, 370.

Ellsworth, W. L., R. H. Campbell, D. P. Hill, R. A. Page, R. W. Alweine, T. C. Hanks, T. H. Heaton, J. A. Hileman, H. Kanamori, B. Minster, and J. H. Whitcomb (1973). Point Mugu, California, earthquake of 21 February 1973 and its aftershocks, *Science* **182**, 1127-1129.

Gawthrop, W. H. (1978). Seismicity and tectonics of the central California coastal region, *Calif. Div. Mines Geology, Special Report* 137, 45-55.

Hauksson, E. (1990). Earthquakes, faulting and stress in the Los Angeles basin, *J. Geophys. Res.* **95**, 15365-15394.

Helmberger, D. V. and G. R. Engen (1980). Modeling the long-period body waves from shallow earthquakes at regional ranges, *Bull. Seism. Soc. Am.* **70**, 1699-1714.

Helmberger, D. V., P. G. Somerville, J. P. McLaren, L. J. Burdick, E. Garnero, A. Bent, and L. S. Zhao (1990). The location and parameters of the Lompoc, California earthquake of November 4, 1927, submitted for publication.

Hornafius, J. S., B. P. Luyendyk, R. R. Terres, and M. J. Kamerling (1986). Timing and extent of Neogene rotation in the western Transverse Ranges, California, *Geol. Soc. Am. Bull.* **97**, 1476-1487.

Hutton, L. K., C. R. Allen, and C. E. Johnson (1985). Seismicity of southern California: Earthquakes of ML 3.0 and greater 1975 through 1983, Seismological Lab., California Institute of Technology, 142 pp.

Langston, C. A. (1978). The February 9, 1971 San Fernando earthquake: a study of source finiteness in teleseismic body waves, *Bull. Seism. Soc. Am* **68**, 1-29.

Langston, C. A. and D. V. Helmberger (1975). A procedure for modelling shallow dislocation sources, *Geophys. J. R. Astr. Soc* **42**, 117-130.

Luyendyk, B. P., M. J. Kamerling, and R. R. Terres (1980). Geometric model for Neogene crustal rotations in southern California, *Geol. Soc. Am. Bull.* **91**, 211-217.

Luyendyk, B. P., M. J. Kamerling, R. R. Terres, and J. S. Hornafius (1985). Simple shear of southern California during Neogene time suggested by paleomagnetic declinations, *J. Geophys. Res.* **90**, 12454-12466.

Steritz, J. W. (1986). The southern termination of the Hosgri fault zone, offshore south-central California, *M. S. Theses*, University of California at Santa Barbara, 78 pp.

Toppozada, T. R., C. R. Real, and D. L. Parke (1981). Preparation of isoseismal maps and summary of reported effects for pre-1900 California earthquakes, *Calif. Div. Mines Geol. Open-File Rept.* 81-11, Sacramento, 182 pp.

Wallace, T. C., D. V. Helmberger, and J. E. Ebel (1981a). A broadband study of the 13 August 1978 Santa Barbara earthquake, *Bull. Seism. Soc. Am* **71**, 1701-1718.

Wallace, T. C., D. V. Helmberger, and G. R. Mellman, (1981b). A technique for the inversion of regional data in source parameter studies, *J. Geophys. Res.* **86**, 1679-1685.

Yerkes, R. F., H. G. Greene, J. C. Tinsley, and K. R. Lajoie (1980). Seismotectonic setting of the Santa Barbara Channel area, southern California, *U. S. Geol. Surv., Open-File Rept.* 80-299, 24 pp.

Zhao, L. S. and D. V. Helmberger (1990). Velocity structure beneath the Tibetan Plateau, *EOS* **71**, 557.

Zhao, L. S., D. V. Helmberger, and D. G. Harkrider (1990). Shear-velocity structures of the crust and upper mantle beneath Tibet and southeastern China, *Geophys. J. R. Astr. Soc.* (in press).

Zoback, M. D., M. L. Zoback, V. S. Mount, J. Suppe, J. P. Eaton, J. H. Healy, D. Oppenheimer, P. Reasenberg, L. Jones, C. B. Raleigh, I. G. Wong, O. Scotti, and C. Wentworth (1987). New evidence on the state of stress of the San Andreas fault system, *Science* **238**, 1105-1111.

SEISMOLOGICAL LABORATORY 252-21
CALIFORNIA INSTITUTE OF TECHNOLOGY
PASADENA, CALIFORNIA 91125

Manuscript received 22 August 1990